Struct Multidisc Optim (2015) 52:1229–1241
DOI 10.1007/s00158-015-1294-0

EDUCATIONAL ARTICLE

Design of materials using topology optimization and energy-based homogenization approach in Matlab

Liang Xia[1] · **Piotr Breitkopf**[1]

Received: 10 April 2014 / Revised: 15 June 2015 / Accepted: 17 June 2015 / Published online: 19 July 2015

Abstract This paper presents a Matlab code for the optimal topology design of materials with extreme properties. For code compactness, an energy-based homogenization approach is adopted rather than the asymptotic approach. The effective constitutive parameters are obtained in terms of element mutual energies. A corresponding solution scheme with periodic boundary conditions is implemented. With a single constraint on material volume fraction, this code allows to maximize or minimize objective functions constituted by homogenized stiffness tensors such as bulk modulus, shear modulus and Poisson's ratio. The complete Matlab code built on top of the 88-line code (Andreassen et al. Struct Multidiscip Optim 43(1):1–16, 2011) is given in the Appendix.

Keywords Topology optimization · Microstructure · Homogenization · Periodic boundary conditions · Matlab

Nomenclature

ϵ	Aspect ratio between the macro and micro scales
η	Numerical damping coefficient
λ	Lagrange multiplier
ρ_e	Element density design variable
ρ_e^{new}	Updated element density variable
$\varepsilon_{pq}^{*(kl)}$	Periodic fluctuation strain fields
$\varepsilon_{pq}^{0(kl)}$	Unit test strain fields
ε_{ij}^{0}	Prescribed strain fields
$\varepsilon_{pq}^{A(kl)}$	Superimposed strain fields
ϑ	Upper bound of volume fraction
B_e	Term obtained from the optimality condition
c	Objective function
d	Spatial dimension
E_{ijkl}^{H}	Homogenized elasticity tensor in index notation
E_{ij}^{H}	Homogenized elasticity tensor in matrix notation
E_0	Solid material Young's modulus
E_e	Element Young's modulus
E_{ijkl}	Elasticity tensor in index notation
E_{min}	Void material Young's modulus (Ersatz material)
m	Design variable move limit
N	Number of finite elements
p	Penalization factor
q_e^{ij}	Element e mutual energy
Q_{ij}	Summed element mutual energies
u	Microscale displacement field
u^*	Microscale periodic fluctuation field
u^ϵ	Macroscale displacement field depending on ϵ
v	Microscale Y-periodic admissible displacement fields
v_e	Element volume
w_i^k	Periodic displacement prescribed on opposite nodes
x	Macroscale cartesian coordinate
Y	Base cell domain
y	Microscale cartesian coordinate
y_j^0	Base cell size in direction j
$\bar{\mathbf{W}}$	Periodic displacement prescribed on the cell
$\mathbf{F}$	External force vector

✉ Liang Xia
liang.xia@utc.fr

[1] Sorbonne universités, Université de Technologie de Compiègne, CNRS, UMR 7337 Roberval, Centre de Recherches de Royallieu, CS 60319, 60203, Compiègne Cedex, France

$\mathbf{K}$	Global stiffness matrix
$\mathbf{k}_0$	Element stiffness matrix with unit Young's modulus
$\mathbf{k}_e$	Element stiffness matrix
$\mathbf{U}$	Global displacement vector
$\mathbf{u}_e^{A(ij)}$	Element displacement vector for load case ij

1 Introduction

Topology optimization (Bendsøe and Kikuchi 1988) was first employed for the material design by Sigmund (1994) via an inverse homogenization approach. This was followed by a series of systematic works (e.g., Sigmund and Torquato 1997; Sigmund 2000; Gibiansky and Sigmund 2000). The subject has been later successively addressed by the density-based approach (e.g., Neves et al. 2000; Guest and Prévost 2007; Zhang et al. 2007), level-set method (e.g., Challis et al. 2008; Wang et al. 2014), topological derivative (e.g., Amstutz et al. 2010), and ESO-type method (e.g., Huang et al. 2011). Figures 1, 2 and 3 show some representative extremal microstructures designed by topology optimization. Functionally graded material and structure designs have been given by Paulino et al. (2009) and Almeida et al. (2010). Another closely related area of research is concurrent material and structural design (e.g., Rodrigues et al. 2002; Zhang and Sun 2006; Xia and Breitkopf 2014a, 2015).

After the 99-line Matlab code in the seminal article by Sigmund (2001), a series of educational papers with compact Matlab implementations have significantly contributed to the popularity and to the development of topology optimization. These include a coupled level set method using the FEMLAB package by Liu et al. (2005), the ESO method by Huang and Xie (2010), the discrete level-set method by Challis (2010), the 199-line code for Pareto-optimal tracing with the aid of topological derivatives by Suresh (2010), the 88-line Matlab code by Andreassen et al. (2011), the Matlab code for the generation of polygonal meshes (PolyMesher) and the topology optimization framework (PolyTop) that are based on Talischi (2012a, b), and a parallel computing implementation (Mahdavi et al. 2006).

The present authors have also benefited from these educational papers, for instance, the multi-component structural system designs (Xia et al. 2012, 2013) are given within the framework of the 99-line code (Sigmund 2001). The reduced multiscale topology optimization (Xia and Breitkopf 2014b) uses the discrete level-set method (Challis 2010). Moreover, the authors' recent work on concurrent material and structural design (Xia and Breitkopf 2014a, 2015) builds on top of the 88-line code framework (Andreassen et al. 2011) along with the ESO optimizer (Huang and Xie 2010).

The present work extends the 88-line code to the optimal design of materials with extreme properties. We follow the design strategy proposed by Sigmund (1994), where the homogenized material constitutive parameters are evaluated in terms of element mutual energies. For effective material property prediction, rather than using the conventional asymptotic expansion (Guedes and Kikuchi 1990), we adopt an equivalent energy-based homogenization approach that employs average stress and strain theorems (Hashin 1983). It will be shown in Section 6 that the applied design algorithm with the Matlab implementation (see the Appendix) can generate extremal microstructures with similar topology configurations as in Figs. 1, 2 and 3.

The remainder of the paper is organized as follows: in Section 2, homogenization theory is briefly reviewed. Section 3 presents the implementation of periodic boundary conditions. Section 4 gives the optimization model. Section 5 explains the Matlab implementation. Section 6 gives several numerical examples using the proposed code. Conclusions are drawn in Section 7. The Matlab implementation is given in the Appendix.

2 Homogenization

Within the scope of linear elasticity, the equivalent constitutive behavior of periodically patterned microstructures (Fig. 4) can be evaluated using the homogenization method (Guedes and Kikuchi 1990). Consider a single cell Y in $\mathbb{R}^3$

$$Y =]0, y_1^0[\times]0, y_2^0[\times]0, y_3^0[, \tag{1}$$

where y_1^0, y_2^0, and y_3^0 are the dimensions of the base cell in the three directions.

Following the asymptotic homogenization, the macroscale displacement field $u^\epsilon(x)$ depending on the

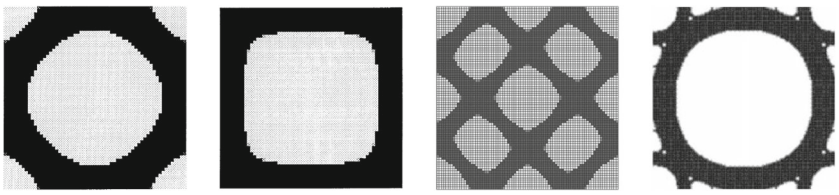

Fig. 1 Microstructures with maximized bulk moduli: the first two from Sigmund (2000), the third from Zhang et al. (2007), the last from Amstutz et al. (2010) (from *left* to *right*)

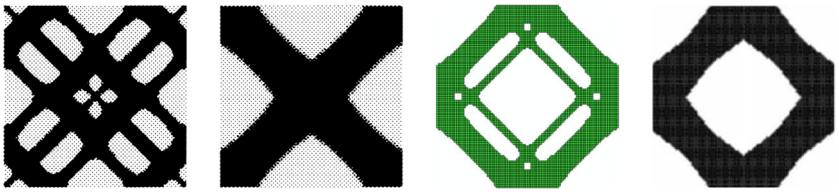

Fig. 2 Microstructures with maximized shear moduli: the first two from Neves et al. (2000), the third from Huang et al. (2011), the last from Amstutz et al. (2010) (from *left* to *right*)

the aspect ratio ϵ between the macro and micro scales is expanded as

$$u^{\epsilon}(x) = u_0(x, y) + \epsilon u_1(x, y) + \epsilon^2 u_2(x, y) \ldots, y = x/\epsilon, \tag{2}$$

where the involved functions are dependent on the global macroscopic variable x and the local microscopic variable y. The dependence on $y = x/\epsilon$ implies that a quantity varies within a very small neighborhood of a macroscopic point x, which may be viewed as "stretching" the microscale so it becomes comparable to the macroscale. When $\epsilon \ll 1$, the dependence on y can be considered periodic for a fixed macroscopic point x.

When only the first order terms of the asymptotic expansion in (2) are considered, the homogenized stiffness tensor E^H_{ijkl} is given by averaging the integral over the the base cell Y as

$$E^H_{ijkl} = \frac{1}{|Y|}\int_Y E_{ijpq}(\varepsilon^{0(kl)}_{pq} - \varepsilon^{*(kl)}_{pq})\mathrm{d}Y, \tag{3}$$

where the Einstein index summation notation is used and $\varepsilon^{*(kl)}_{pq}$ is the Y-periodic solution of

$$\int_Y E_{ijpq}\varepsilon^{*(kl)}_{pq}\frac{\partial v_i}{\partial y_j}\mathrm{d}Y = \int_Y E_{ijpq}\varepsilon^{0(kl)}_{pq}\frac{\partial v_i}{\partial y_j}\mathrm{d}Y, \tag{4}$$

where v is Y-periodic admissible displacement field and $\varepsilon^{0(kl)}_{pq}$ corresponds to the three (2D) or six (3D) linearly independent unit test strain fields.

With the intention of presenting a compact Matlab code, the energy-based approach which employs average stress and strain theorems is adopted in this work instead of the asymptotic approach. The energy-based approach imposes the unit test strains directly on the boundaries of the base cell, inducing $\varepsilon^{A(kl)}_{pq}$ which corresponds to the superimposed strain fields $(\varepsilon^{0(kl)}_{pq} - \varepsilon^{*(kl)}_{pq})$ in (3). According to Hashin (1983), these are two equivalent approaches for the prediction of material effective properties. A detailed implementation of periodic boundary conditions is given in Section 3.

With the intension to favor effective existing algorithms used in topology optimization, (3) is rewritten in an equivalent form in terms of element mutual energies (Sigmund 1994)

$$E^H_{ijkl} = \frac{1}{|Y|}\int_Y E_{pqrs}\varepsilon^{A(ij)}_{pq}\varepsilon^{A(kl)}_{rs}\mathrm{d}Y. \tag{5}$$

In finite element analysis, the base cell is discretized into N finite elements and (5) is approximated by

$$E^H_{ijkl} = \frac{1}{|Y|}\sum_{e=1}^{N}(\mathbf{u}^{A(ij)}_e)^T\mathbf{k}_e\mathbf{u}^{A(kl)}_e, \tag{6}$$

where $\mathbf{u}^{A(kl)}_e$ are the element displacement solutions corresponding to the unit test strain fields $\boldsymbol{\varepsilon}^{0(kl)}$, and $\mathbf{k}_e$ is the element stiffness matrix. In 2D cases, we note that $11 \rightarrow 1$, $22 \rightarrow 2$, and $12 \rightarrow 3$, allowing to write (6) in an expanded form

$$\begin{bmatrix} E^H_{11} & E^H_{12} & E^H_{13} \\ E^H_{21} & E^H_{22} & E^H_{23} \\ E^H_{31} & E^H_{32} & E^H_{33} \end{bmatrix} = \begin{bmatrix} Q_{11} & Q_{12} & Q_{13} \\ Q_{21} & Q_{22} & Q_{23} \\ Q_{31} & Q_{32} & Q_{33} \end{bmatrix}, \tag{7}$$

where the terms Q_{ij}

$$Q_{ij} = \frac{1}{|Y|}\sum_{e=1}^{N} q^{(ij)}_e, \tag{8}$$

are the sums of element mutual energies $q^{(ij)}_e$

$$q^{(ij)}_e = (\mathbf{u}^{A(i)}_e)^T\mathbf{k}_e\mathbf{u}^{A(j)}_e. \tag{9}$$

3 Periodic boundary conditions (PBC)

The strain fields $\varepsilon^{A(kl)}_{pq}$ in (5) are evaluated by solving the base cell equilibrium problem subjected to the unit test strains $\varepsilon^{0(kl)}_{pq}$. Under the assumption of periodicity, the displacement field of the base cell subjected to a given strain

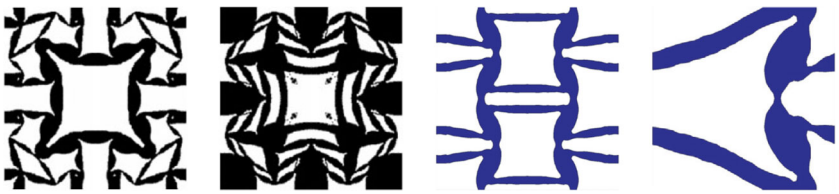

Fig. 3 Microstructures with minimized negative Poisson's ratios: the first two from Amstutz et al. (2010), the last two from Wang et al. (2014) (from *left* to *right*)

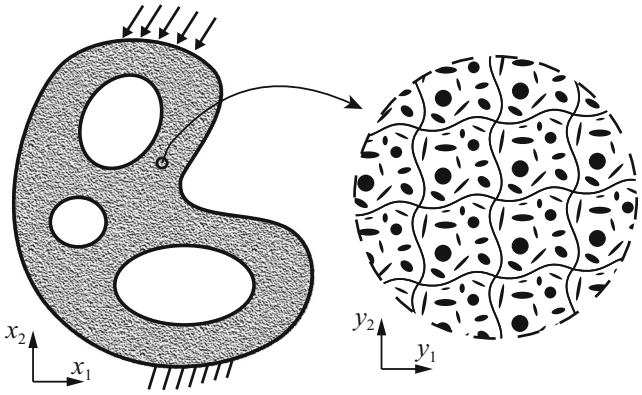

Fig. 4 Illustration of a material point constituted by periodically patterned microstructures

ε_{ij}^0 can be written as the sum of a macroscopic displacement field and a periodic fluctuation field u_i^* (Michel et al. 1999)

$$u_i = \varepsilon_{ij}^0 y_j + u_i^*. \tag{10}$$

In practice, (10) cannot be directly imposed on the boundaries because the periodic fluctuation term u_i^* is unknown. This general expression needs to be transformed into a certain number of explicit constraints between the corresponding pairs of nodes on the opposite surfaces of the base cell (Xia et al. 2003). Consider a 2D base cell as shown in Fig. 5, the displacements on a pair of opposite boundaries are

$$\begin{cases} u_i^{k+} = \varepsilon_{ij}^0 y_j^{k+} + u_i^* \\ u_i^{k-} = \varepsilon_{ij}^0 y_j^{k-} + u_i^*, \end{cases} \tag{11}$$

where superscripts "$k+$" and "$k-$" denote the pair of two opposite parallel boundary surfaces that are oriented perpendicular to the k-th direction ($k = 1, 2, 3$). The periodic term u_i^* can be eliminated through the difference between the displacements

$$u_i^{k+} - u_i^{k-} = \varepsilon_{ij}^0 (y_j^{k+} - y_j^{k-}) = \varepsilon_{ij}^0 \Delta y_j^k. \tag{12}$$

For any given parallelepiped base cell model, Δy_j^k is constant. In the case of Fig. 5, we have $\Delta y_1^1 = y_1^0$, $\Delta y_2^1 = 0$ and $\Delta y_1^2 = 0$, $\Delta y_2^2 = y_2^0$. Thus, with a specified ε_{ij}^0, the right-hand side becomes a constant

$$u_i^{k+} - u_i^{k-} = w_i^k, \tag{13}$$

since $w_i^k = \varepsilon_{ij}^0 \Delta y_j^k$. This form of boundary conditions can be directly imposed in the finite element model by constraining the corresponding pairs of nodal displacements. At the same time, this form of boundary conditions meets the periodicity and the continuity requirements for both displacement as well as stress when using displacement-based finite element analysis (Xia et al. 2006).

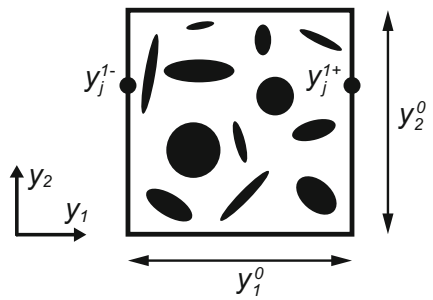

Fig. 5 A 2D rectangular base cell model

4 Optimization model

4.1 Modified SIMP approach

The base cell is discretized into N finite elements and the same number of density design variables $\boldsymbol{\rho} \in \mathbb{R}^N$ are correspondingly defined. Using the modified SIMP approach (Sigmund 2007), the element Young's modulus E_e is defined as

$$E_e(\rho_e) = E_{min} + \rho_e^p (E_0 - E_{min}), \tag{14}$$

where E_0 is the Young's modulus of solid material and E_{min} is the Young's modulus of the Ersatz material, which is an approximation for void material using compliant material (Allaire et al. 2004) to prevent the singularity of the stiffness matrix. ρ_e takes values between 0 and 1, with these limits corresponding to the Ersatz and solid materials respectively. p is a penalization factor introduced to drive the density distribution closer towards the so-called black-and-white solution.

The mathematical formulation of the optimization problem reads as follows

$$\begin{aligned} \min_{\boldsymbol{\rho}} &: c(E_{ijkl}^H(\boldsymbol{\rho})) \\ \text{s.t.} &: \mathbf{K}\mathbf{U}^{A(kl)} = \mathbf{F}^{(kl)}, k, l = 1, \ldots, d \\ &: \textstyle\sum_{e=1}^N v_e \rho_e / |Y| \le \vartheta \\ &: 0 \le \rho_e \le 1, e = 1, \ldots, N \end{aligned} \tag{15}$$

where $\mathbf{K}$ is the global stiffness matrix, $\mathbf{U}^{A(kl)}$ and $\mathbf{F}^{(kl)}$ are the global displacement vector and the external force vector of the test case (kl) respectively. d is the spatial dimension, v_e denotes the element volume, and ϑ is the upper bound on the volume fraction. The objective $c(E_{ijkl}^H)$ is a function of the homogenized stiffness tensors. For instance, in the 2D case, the maximization of the material bulk modulus corresponds to the minimization of

$$c = -\left(E_{1111} + E_{1122} + E_{2211} + E_{2222}\right), \tag{16}$$

and the maximization of material shear modulus corresponds to the minimization of

$$c = -E_{1212}. \tag{17}$$

4.2 Numerical solution of the homogenization equations

When both the geometry and the loading exhibit symmetries, which is the case here, the periodic boundary conditions presented in Section 3 can be simplified to conventional boundary conditions (Hassani and Hinton 1998b). To keep the derivations general, such simplification is not applied in the present work. Instead, the periodic boundary conditions are imposed in a direct manner (see Section 3). With regard to the finite element solution of (13), the direct solution scheme eliminating the redundant unknowns is adopted here. Note that, apart from the direct solution scheme, there exist two other types of solution schemes using penalty methods and Lagrange multipliers (Michel et al. 1999).

Separating the global displacement vector $\mathbf{U}$ into four parts: $\bar{\mathbf{U}}_1$ denotes the prescribed displacement values, $\mathbf{U}_2$ denotes the unknowns corresponding to the interior nodes, $\mathbf{U}_3$ and $\mathbf{U}_4$ denote unknowns corresponding to the nodes located on the opposite boundaries of the base cell satisfying $\mathbf{U}_4 = \mathbf{U}_3 + \bar{\mathbf{W}}$, where $\bar{\mathbf{W}}$ is a prescribed value computed via a given $\boldsymbol{\varepsilon}^{0(kl)}$ according to (13). The equilibrium equation in (15) can be expanded to

$$\begin{bmatrix} \mathbf{K}_{11} & \mathbf{K}_{12} & \mathbf{K}_{13} & \mathbf{K}_{14} \\ \mathbf{K}_{21} & \mathbf{K}_{22} & \mathbf{K}_{23} & \mathbf{K}_{24} \\ \mathbf{K}_{31} & \mathbf{K}_{32} & \mathbf{K}_{33} & \mathbf{K}_{34} \\ \mathbf{K}_{41} & \mathbf{K}_{42} & \mathbf{K}_{43} & \mathbf{K}_{44} \end{bmatrix} \begin{bmatrix} \bar{\mathbf{U}}_1 \\ \mathbf{U}_2 \\ \mathbf{U}_3 \\ \mathbf{U}_4 \end{bmatrix} = \begin{bmatrix} \mathbf{F_1} \\ \mathbf{F_2} \\ \mathbf{F_3} \\ \mathbf{F_4} \end{bmatrix}, \tag{18}$$

where $\mathbf{F}_1$ is an unknown vector and equals to the reaction forces at the nodes with prescribed displacements, $\mathbf{F}_2 = \mathbf{0}$, and $\mathbf{F_3} + \mathbf{F_4} = \mathbf{0}$ due to the periodicity assumption. Note that $\mathbf{K}$ is symmetric, i.e. $\mathbf{K}_{ij} = \mathbf{K}_{ji}$ in (18). Eliminating the first row, adding the third and fourth rows, and using the relationship $\mathbf{U}_4 = \mathbf{U}_3 + \bar{\mathbf{W}}$, (18) reduces to

$$\begin{aligned} &\begin{bmatrix} \mathbf{K}_{22} & \mathbf{K}_{23} + \mathbf{K}_{24} \\ sym. & \mathbf{K}_{33} + \mathbf{K}_{34} + \mathbf{K}_{43} + \mathbf{K}_{44} \end{bmatrix} \begin{bmatrix} \mathbf{U}_2 \\ \mathbf{U}_3 \end{bmatrix} \\ &= -\begin{bmatrix} \mathbf{K}_{21} \\ \mathbf{K}_{31} + \mathbf{K}_{41} \end{bmatrix} \bar{\mathbf{U}}_1 - \begin{bmatrix} \mathbf{K}_{24} \\ \mathbf{K}_{34} + \mathbf{K}_{44} \end{bmatrix} \bar{\mathbf{W}}. \end{aligned} \tag{19}$$

and allows for the solution of the system.

4.3 Optimality criteria method

Once the displacement solution is obtained, the optimization problem (15) is solved by means of a standard optimality criteria method. Following (Bendsøe and Sigmund 2003), the heuristic updating scheme is formulated as

$$\rho_e^{\text{new}} = \begin{cases} \max(0,\, \rho_e - m) & \text{if } \rho_e B_e^{\eta} \le \max(0,\, \rho_e - m) \\ \min(1,\, \rho_e + m) & \text{if } \rho_e B_e^{\eta} \ge \min(1,\, \rho_e + m) \\ \rho_e B_e^{\eta} & \text{otherwise,} \end{cases} \tag{20}$$

where m is a positive move limit, η is a numerical damping coefficient, and B_e is obtained from the optimality condition as (Bendsøe and Sigmund 2003)

$$B_e = \frac{-\frac{\partial c}{\partial \rho_e}}{\lambda \frac{\partial V}{\partial \rho_e}}, \tag{21}$$

where the Lagrange multiplier λ is chosen by means of a bisection algorithm to enforce the satisfaction of the constraint on material volume fraction. The sensitivity of the objective function $\partial c/\partial \rho_e$ is computed using the adjoint method (Bendsøe and Sigmund 2003)

$$\frac{\partial E_{ijkl}^H}{\partial \rho_e} = \frac{1}{|Y|} p \rho_e^{p-1} (E_0 - E_{min}) (\mathbf{u}_e^{A(ij)})^T \mathbf{k}_0 \mathbf{u}_e^{A(kl)}, \tag{22}$$

in accordance with the objective definition, where $\mathbf{k}_0$ is the element stiffness matrix for an element with unit Young's modulus. When a uniform mesh is used, the element volume v_e is set to 1 and therefore $\partial V/\partial \rho_e = 1$.

In order to ensure the existence of the solution to the optimization problem (15), sensitivity and density filtering schemes are used following (Andreassen et al. 2011) to avoid the formation of checkerboard pattern and the mesh-dependency issue.

5 Matlab implementation

In this section the Matlab code (see Appendix) is explained. The present code is built on top of the 88-line code (Andreassen et al. 2011). The first 38 lines are left unchanged. Material properties are defined in lines 4 to 6. The element stiffness matrix and the corresponding nodal informations are defined in lines 8 to 17. Matrices that are to be used for sensitivity and density filtering are predefined in lines 19 to 38. The design domain is assumed to be rectangular and discretized into square plane stress elements. The main program is called from the Matlab prompt by the command

```
topX(nelx,nely,volfrac,penal,rmin,ft)
```

where `nelx` and `nely` denote the number of elements along the horizontal and vertical directions respectively,

`volfrac` is the prescribed volume fraction, `penal` is the penalization factor p, `rmin` is the filter radius, and `ft` specifies whether sensitivity filtering (`ft=1`) or density filtering (`ft=2`) is to be used.

The following subsections present the original parts of code developed in the scope of the current work. Apart from these, two minor changes are made to the original 88-line code: line 103, the stop condition is set to `1e-9` to enforce the satisfaction of the volume fraction constraint; line 111, `mean(xPhys(:))` is used for programming consistency.

5.1 Lines 39–56: periodic boundary conditions

Periodic boundary conditions (Section 3) are defined in lines 39 to 56. `e0` defines the three unit test strain fields. The base cell shown in Fig. 6 is discretized into 3×3 elements for the purpose of illustration. The degrees of freedom (DOFs) are divided into four sets as presented in (18)

$$\begin{cases} \texttt{d1} = \{7, 8, 31, 32, 25, 26, 1, 2\} \\ \texttt{d15} = \{11, 12, 13, 14, 19, 20, 21, 22\} \\ \texttt{d3} = \{3, 4, 5, 6, 15, 16, 23, 24\} \\ \texttt{d4} = \{27, 28, 29, 30, 9, 10, 17, 18\}, \end{cases} \tag{23}$$

where `d1` contains the DOFs of the four corner points (A, B, C, D), `d3` contains the DOFs on the left and bottom boundaries except the corner DOFs, `d4` contains the DOFs on the right and top boundaries except the corner DOFs, and `d2` contains the remaining inner DOFs. In practice, one has to fix at least one node to avoid rigid body motion when solving the PBC problem. When point A is chosen to be fixed, points B, C, D are prescribed with values corresponding to the three unit test strain fields computed according to (13) in lines 51 to 55. `wfixed` in line 56 corresponds to w_i^k in (13) and $\bar{\mathbf{W}}$ in (19), is the constant difference vector between the DOFs of `d3` and `d4`.

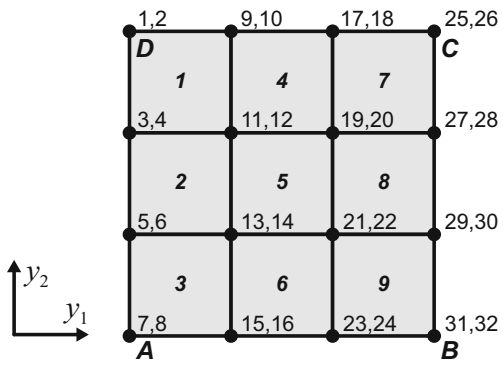

Fig. 6 A base cell discretized into 3×3 elements

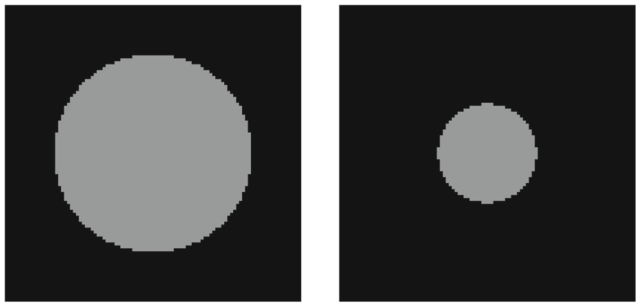

Fig. 7 Two initial guess topologies for a 100×100 base cell

5.2 Lines 57–71: initialization

In the 2D case, the base cell model needs to be evaluated three times corresponding to the three unit test strain fields. Lines 58–60 preallocate three cells `qe`, `Q` and `dQ` to store the element mutual energies, the summed mutual energies, and the sensitivities of the summed mutual energies.

Lines 61–69 give the initial guess of material topology layout (the left figure in Fig. 7). In structural compliance minimization designs (Sigmund 2001), the initial guess usually consists of a uniformly distributed density field to avoid local minimum designs. However, this cannot be employed for material designs because the applied periodic boundary conditions would result in a uniformly distributed sensitivity field, thus making the variable update impossible. The influence of an initial guess on the final designs has been thoroughly discussed in Sigmund and Torquato (1997), Sigmund (2000), and Gibiansky and Sigmund (2000), however the specific initial guesses are not provided. Following Amstutz et al. (2010), we simply define a circular region with softer material at the center of the base cell as shown in Fig. 7.

5.3 Lines 76–93: finite element solution, objective and sensitivity analysis

The system in (19) is assembled and solved in lines 76–81. Cells `qe`, `Q`, and `dQ` are evaluated in lines 83–90. Line 91 calculates the objective function in (16) for the maximization of material bulk modulus. Sensitivities are computed lines 92 and 93, and stored in `dc` and `dv`.

6 Illustrative examples

As discussed by Sigmund and Torquato (1997), Sigmund (2000) and Gibiansky and Sigmund (2000), topology optimization design of materials with extreme properties allows for multiple local minima. The initial guess of material

topology layout, the shape of base cell, filter radius, penalization factor and other parameters all have influence on the design solution. In the following examples, we show how to use the present Matlab code to design materials with extreme properties. All of the following tests are performed using Matlab 8.4.0.150421 (R2014b).

6.1 Material bulk modulus maximization

According to Bendsøe and Sigmund (2003), the so-called one-length scale microstructures can be obtained by setting the filter radius to a comparatively large value, saying 10 % of the cell length at the beginning iterations, then gradually decease its value during the optimization process. Here, we simply set the filter radius to 5. The penalization factor is set to 3. Materials with maximized bulk moduli shown in Fig. 8 can be obtained by calling

```
topX(100,100,0.5,3,5,1)
```

and

```
topX(100,100,0.5,3,5,2)
```

respectively. Both filtering schemes converge after around 200 iterations, however the sensitivity filtering scheme fails in giving a clear structural layout.

To favor solutions with clearly discernible topologies, Bendsøe and Sigmund (2003) proposed to gradually increase the penalization factor during the optimization process. Note that the topology may be driven closer towards a black-white solution if the penalization value is increased. It should be noted however, that the problem in (15) is non-convex for values of $p > 1$. Thus, while high penalization values will result in cleaner topologies, the algorithm is more likely to get trapped in a local minimum.

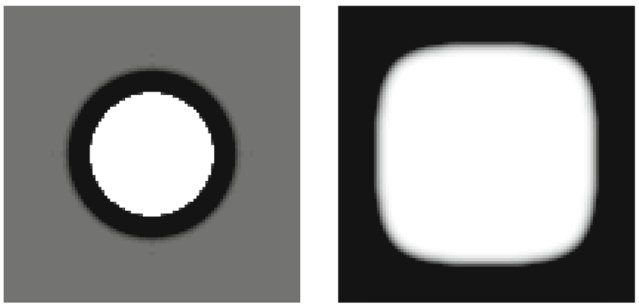

Fig. 8 Materials with maximized bulk moduli obtained using sensitivity filtering (*left*, $c = -0.4388$, iteration 163) and density filtering (*right*, $c = -0.6537$, iteration 216) with penalty factor $p = 3$ and filter radius $r = 5$

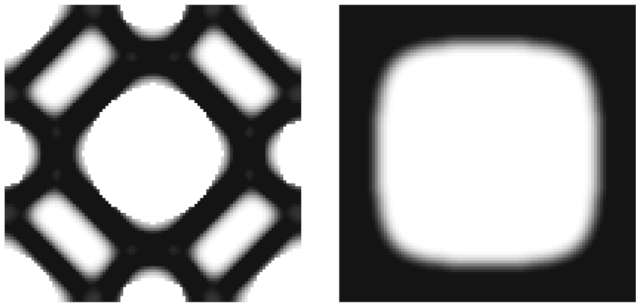

Fig. 9 Materials with maximized bulk moduli obtained using sensitivity filtering (*left*, $c = -0.5636$, iteration 269) and density filtering (*right*, $c = -0.6207$, iteration 160) with penalty factor $p = 5$ and filter radius $r = 5$

In this work, the penalization factor is set as a constant value, thus we simply increase the value to 5. Recalling

```
topX(100,100,0.5,5,5,1)
```

and

```
topX(100,100,0.5,5,5,2)
```

respectively, we obtain materials shown in Fig. 9. It can be observed that the increased penalization value results in clearer topology layout in the case of sensitivity filtering, while has little influence in the case of density filtering.

Similar to the implementation of penalization, filtering scheme is applied here to regularize the problem in (15), that means a smaller filter radius will result in a better solution because higher frequency details are allowed by the low-pass filer, thus enriching the solution. To show the influence of the filter radius on the solutions, the same problem is solved again with filter radius $r = 2$ by calling

```
topX(100,100,0.5,5,2,1)
```

Fig. 10 Materials with maximized bulk moduli obtained using sensitivity filtering (*left*, $c = -0.6793$, iteration 183) and density filtering (*right*, $c = -0.6540$, iteration 129) with penalty factor $p = 5$ and filter radius $r = 2$

and

```
topX(100,100,0.5,5,2,2)
```

respectively. As shown in Fig. 10, the decreased filter radius value results in a more detailed microstructure when using sensitivity filtering, while a slightly varied microsctructure in the case of density filtering. As expected, both materials in Fig. 10 possess higher bulk moduli than those in Fig. 9 due to the decreased filter radius value.

We note that when using sensitivity filtering (left figure in Fig. 8) the minimum is obtained at iteration 10, after which the algorithm diverges. This is a common phenomenon for all the following tests when using sensitivity filtering. Sensitivity filtering scheme is fully heuristic in nature and was developed for the specific case of compliance minimization (Sigmund 2001). Thus, there is no guarantee it will perform well for material designs. In the contrary, density filtering scheme does not suffer from the concerned issue and has more robust performances according to Figs. 8, 9, and 10. Therefore, density filtering scheme is in general more preferable for the design of material microstructures.

The present Matlab code also allows the design of rectangular base cells. The two rectangular microstructures shown in Fig. 11 are obtained by calling

```
topX(150,100,0.5,5,2,1)
```

Fig. 11 Materials with maximized bulk moduli obtained using sensitivity filtering (*top*, $c = -0.6730$, iteration 345) and density filtering (*bottom*, $c = -0.6317$, iteration 349) with penalty factor $p = 5$ and filter radius $r = 2$

and

```
topX(150,100,0.5,5,2,2)
```

using sensitivity filtering and density filtering respectively. Again, it can be observed that a small value for the filter radius results in a more detailed microstructure in the case sensitivity filtering is used.

From these results, it can be argued that the results obtained using density filtering are less sensitive to the choice of optimization parameters such as penalization factor and filter radius.

6.2 Material shear modulus maximization

To design materials with maximized shear moduli, one may simply replace lines 91 and 92 of the code by

```
c=-Q(3,3);
dc=-dQ{3,3};
```

and the corresponding designs in Fig. 12 can be obtained by calling

```
topX(100,100,0.5,3,5,1)
```

and

```
topX(100,100,0.5,3,5,2)
```

respectively. Compared to the maximization of material bulk modulus, material shear modulus maximization design is less sensitive to the choice of filtering scheme and does not require a high penalization factor to enforce topologically clear designs.

Replacing `min(nelx,nely)/3` by `min(nelx, nely)/6` in line 64, we consider another initial guess with a smaller circular region at the center of the base cell (the right figure in Fig. 7). With the modified initial guess, the

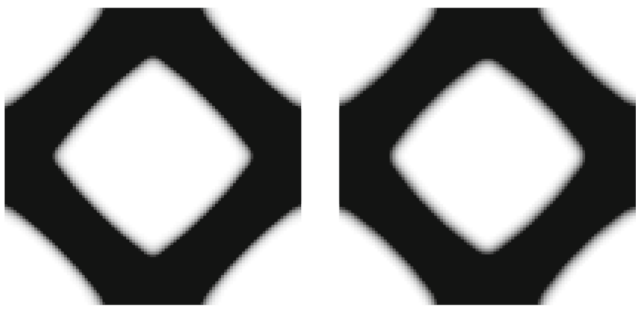

Fig. 12 Materials with maximized shear moduli obtained using sensitivity filtering (*left*, $c = -0.1256$, iteration 12) and density filtering (*right*, $c = -0.1213$, iteration 72) with penalty factor $p = 3$ and filter radius $r = 5$

same function calls result in different material topology designs in Fig. 13. The difference between the results in Figs. 12 and 13 indicates that the choice of initial material topology guess has an severe influence on the final designs. As argued by Bendsøe and Sigmund (2003), different initial guesses may lead to different microstructures which may possess similar material properties due to the non-uniqueness of the solution. Sometimes the microstructural topologies obtained from different initial guesses are in fact the shifted versions of the same topology. It is also suggested to start with an old design to a similar problem, which may save considerable amount of computing time as can be seen from a recent work by Andreassen et al. (2014) for 3D material designs with negative Poisson ratio.

By decreasing the convergence criterion from 0.01 to 0.001, i.e, replacing line 73 by

```
while (change > 0.001)
```

materials with higher shear moduli as shown in Fig. 14 can be achieved by the same function calls as above while requiring more design iterations. Discussion on this topology transition has been given in a recent review paper (Sigmund and Maute 2013) that "The optimization rapidly finds a fairly good design but requires a very large number of iterations for just slight improvements in objective function but rather large changes in geometry." (page 1045), and "To the best of our knowledge remedies for this issues are unknown and we pose it as a challenge to the community to come up with more efficient updates for continuous variable approaches." (page 1046).

6.3 Materials with negative Poisson's ratio

The design of materials with negative Poisson's ratio $\mu = \frac{E_{1122}}{E_{1111}}$ using topology optimization is a challenging subject. As shown by Sigmund (1994), the construction of negative

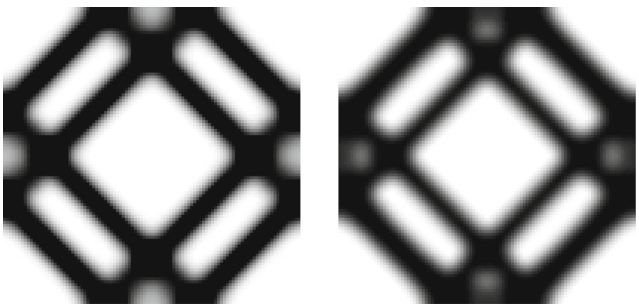

Fig. 13 Materials with maximized shear moduli obtained from a modified initial guess using sensitivity filtering (*left*, $c = -0.1118$, iteration 58) and density filtering (*right*, $c = -0.1043$, iteration 64) with penalty factor $p = 3$ and filter radius $r = 5$

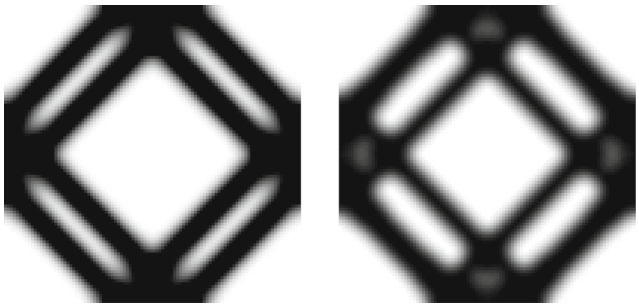

Fig. 14 Materials with maximized shear moduli obtained from the modified initial guess using sensitivity filtering (*left*, $c = -0.1175$, iteration 179) and density filtering (*right*, $c = -0.1057$, iteration 734) with the convergence criterion set as 0.001, penalty factor $p = 3$ and filter radius $r = 5$

Poisson's ratio materials with the present model using an OC-type optimizer is difficult. Successful design of negative Poisson's ratio materials requires imposing additional constraints for instance on isotropy or on bulk modulus. In order to consider multiple constraints in the design, one can either use a specially developed OC-type method (Yin and Yang 2001)), or employ more versatile mathematical programming optimizers such as the method of moving asymptotes (MMA) (Svanberg 1987) implemented by Bendsøe and Sigmund (2003) and more recently by Andreassen et al. (2014) and Wang et al. (2014).

In order to construct negative Poisson's ratio materials with the present model, we propose to define a relaxed form of objective function

$$c = E_{1122} - \beta^l (E_{1111} + E_{2222}), \tag{24}$$

where $\beta \in (0, 1)$ is a fixed parameter defined by the user and exponential l is the design iteration number. With this objective function, optimizer tends to maximize material horizontal and vertical stiffness moduli at the beginning iterations. When the optimization process advances, i.e., l increases, optimizer tends to minimize the value of E_{1122} such that materials with negative Poisson's ratios are constructed.

Choosing $\beta = 0.8$, one need to replace lines 91 and 92 of the Matlab code by

```
c = Q(1,2)-(0.8^loop)*(Q(1,1)+Q(2,2));
dc = dQ{1,2}-(0.8^loop)*(dQ{1,1}+dQ{2,2});
```

and modify line 105 to

```
xnew = max(0,max(x-move,min(1,...
        min(x+move,x.*(-dc./dv/lmid)))));
```

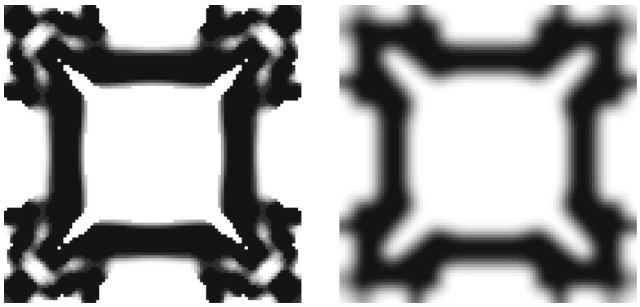

Fig. 15 Materials with negative Poisson's ratio obtained using sensitivity filtering (*left*, $\mu = -0.346$, *volumefraction* $= 0.5$, not converged) and density filtering (*right*, $\mu = -0.239$, *volumefraction* $= 0.437$, not converged) with penalty factor $p = 3$ and filter radius $r = 5$

omitting the numerical damping coefficient. The damping coefficient has to be removed here because both positive and negative sensitivities appear when the objective function of (24) is considered. The constraint on the material volume fraction may not be active during the optimization process as can be seen from the following tests. Design solutions are more sensitive to the choice of the initial guess and other parameters as compared to the previous two cases. As the numerical damping coefficient is removed, the move limit is decreased from 0.2 to 0.1 to stabilize the algorithm, i.e., modifying line 102 to

```
l1=0; l2=1e9; move = 0.1;
```

With all these modifications to the Matlab code, calling

```
topX(100,100,0.5,3,5,1)
```

and

```
topX(100,100,0.5,3,5,2)
```

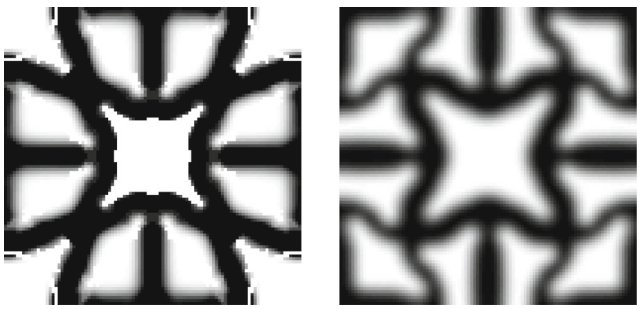

Fig. 16 Materials with negative Poisson's ratio obtained from a modified initial guess using sensitivity filtering (*left*, $\mu = -0.323$, *volumefraction* $= 0.5$, not converged) and density filtering (*right*, $\mu = -0.448$, *volumefraction* $= 0.5$, iteration 113) with penalty factor $p = 3$ and filter radius $r = 5$

results in the materials with negative Poisson's ratio as shown Fig. 15. Note that neither result of the two shown in Fig. 15 is a converged solution. When employing sensitivity filtering scheme, the design process oscillates between two topologies after around 40 iterations and after around 30 iterations in the case of density filtering. The volume fraction constraint is not active in the case of density filtering, which implies that the solution reached a stable state where any addition of material results in a worse topology (*volumefraction* $= 0.437$). Theoretically speaking, the Lagrange multiplier λ in (21) should equal zero within this context. A zero-valued Lagrange multiplier would trigger a division by zero error in the OC update scheme. This is fortunately avoided thanks to an unintentional particularity of the bisection algorithm used to find this Lagrange multiplier: the lowest value it could ever take is $\lambda_{min} \approx (10^{-9} - 0)/2 = 5 \times 10^{-10}$, thus allowing the algorithm to continue.

As in Section 6.2, we consider an alternative initial guess (the right figure in Fig. 7). Substituting `min(nelx,nely)/6` in line 64, the same function calls result in the designs shown in Fig. 16. The left figure in Fig. 16 is one of the two states when oscillation begins after around 50 iterations when using sensitivity filtering. The right figure in Fig. 16 with Poisson's ratio $\mu = -0.446$ is a converged solution at iteration 113 when using density filtering, where note that the volume fraction constraint is satisfied. It is shown by this example that the OC-type optimizer is able to generate well-designed negative Poisson's ratio materials without defining additional constraints provided that the tuning parameters are carefully adjusted.

7 Conclusions

This paper extends the 88-line code (Andreassen et al. 2011) to the design of materials with extreme properties. The adoption of an energy-based homogenization approach instead of the asymptotic approach significantly simplifies the numerical implementation. Periodic boundary conditions and the elimination of the redundant unknowns are presented in detail together with the corresponding numerical implementation.

The present code uses an OC-type optimizer with a single constraint on volume fraction and is able to design materials with extreme bulk and shear modulus. With a proposed relaxed objective function (24), the present code also allows to construct materials with negative Poisson's ratio without introducing additional constraints such as symmetry or on isotropy.

Note that the discussions on the influence of the optimization parameters and the filtering schemes on the

solutions in the present work are mostly based on pure observations. More rigorous explanations would require further investigations.

Acknowledgments The authors highly acknowledge the proposals provided by the anonymous reviewers who helped to improve the quality of the paper. This work was carried out in the framework of the Labex MS2T, which was funded by the French Government, through the program "Investments for the future" managed by the National Agency for Research (Reference ANR-11-IDEX-0004-02). This work is also funded by the China Scholarship Council (CSC).

Appendix: Matlab code

```
%% PERIODIC MATERIAL MICROSTRUCTURE DESIGN
function topX(nelx,nely,volfrac,penal,rmin,ft)
%% MATERIAL PROPERTIES
E0 = 1;
Emin = 1e-9;
nu = 0.3;
%% PREPARE FINITE ELEMENT ANALYSIS
A11 = [12 3 -6 -3; 3 12 3 0; -6 3 12 -3; -3 0 -3 12];
A12 = [-6 -3 0 3; -3 -6 -3 -6; 0 -3 -6 3; 3 -6 3 -6];
B11 = [-4 3 -2 9; 3 -4 -9 4; -2 -9 -4 -3; 9 4 -3 -4];
B12 = [ 2 -3 4 -9; -3 2 9 -2; 4 9 2  3; -9 -2 3 2];
KE = 1/(1-nu^2)/24*([A11 A12;A12' A11]+nu*[B11 B12;B12' B11]);
nodenrs = reshape(1:(1+nelx)*(1+nely),1+nely,1+nelx);
edofVec = reshape(2*nodenrs(1:end-1,1:end-1)+1,nelx*nely,1);
edofMat = repmat(edofVec,1,8)+repmat([0 1 2*nely+[2 3 0 1] -2 -1],nelx*nely,1);
iK = reshape(kron(edofMat,ones(8,1))',64*nelx*nely,1);
jK = reshape(kron(edofMat,ones(1,8))',64*nelx*nely,1);
%% PREPARE FILTER
iH = ones(nelx*nely*(2*(ceil(rmin)-1)+1)^2,1);
jH = ones(size(iH));
sH = zeros(size(iH));
k = 0;
for i1 = 1:nelx
  for j1 = 1:nely
    e1 = (i1-1)*nely+j1;
    for i2 = max(i1-(ceil(rmin)-1),1):min(i1+(ceil(rmin)-1),nelx)
      for j2 = max(j1-(ceil(rmin)-1),1):min(j1+(ceil(rmin)-1),nely)
        e2 = (i2-1)*nely+j2;
        k = k+1;
        iH(k) = e1;
        jH(k) = e2;
        sH(k) = max(0,rmin-sqrt((i1-i2)^2+(j1-j2)^2));
      end
    end
  end
end
H = sparse(iH,jH,sH);
Hs = sum(H,2);
%% PERIODIC BOUNDARY CONDITIONS
e0 = eye(3);
ufixed = zeros(8,3);
U = zeros(2*(nely+1)*(nelx+1),3);
alldofs = (1:2*(nely+1)*(nelx+1));
n1 = [nodenrs(end,[1,end]),nodenrs(1,[end,1])];
d1 = reshape([(2*n1-1);2*n1],1,8);
n3 = [nodenrs(2:end-1,1)',nodenrs(end,2:end-1)];
d3 = reshape([(2*n3-1);2*n3],1,2*(nelx+nely-2));
n4 = [nodenrs(2:end-1,end)',nodenrs(1,2:end-1)];
d4 = reshape([(2*n4-1);2*n4],1,2*(nelx+nely-2));
d2 = setdiff(alldofs,[d1,d3,d4]);
for j = 1:3
  ufixed(3:4,j) =[e0(1,j),e0(3,j)/2;e0(3,j)/2,e0(2,j)]*[nelx;0];
  ufixed(7:8,j) = [e0(1,j),e0(3,j)/2;e0(3,j)/2,e0(2,j)]*[0;nely];
  ufixed(5:6,j) = ufixed(3:4,j)+ufixed(7:8,j);
end
wfixed = [repmat(ufixed(3:4,:),nely-1,1); repmat(ufixed(7:8,:),nelx-1,1)];
%% INITIALIZE ITERATION
qe = cell(3,3);
Q = zeros(3,3);
dQ = cell(3,3);
x = repmat(volfrac,nely,nelx);
for i = 1:nelx
  for j = 1:nely
    if sqrt((i-nelx/2-0.5)^2+(j-nely/2-0.5)^2) < min(nelx,nely)/3
      x(j,i) = volfrac/2;
    end
  end
end
xPhys = x;
change = 1;
loop = 0;
%% START ITERATION
while (change > 0.01)
  loop = loop+1;
  %% FE-ANALYSIS
  sK = reshape(KE(:)*(Emin+xPhys(:)'.^penal*(E0-Emin)),64*nelx*nely,1);
  K = sparse(iK,jK,sK); K = (K+K')/2;
  Kr = [K(d2,d2), K(d2,d3)+K(d2,d4); K(d3,d2)+K(d4,d2), K(d3,d3)+K(d4,d3)+K(d3,d4)+K(d4,d4)];
  U(d1,:) = ufixed;
  U([d2,d3],:) = Kr\(-[K(d2,d1); K(d3,d1)+K(d4,d1)]*ufixed-[K(d2,d4); K(d3,d4)+K(d4,d4)]*wfixed);
  U(d4,:) = U(d3,:)+wfixed;
  %% OBJECTIVE FUNCTION AND SENSITIVITY ANALYSIS
  for i = 1:3
    for j = 1:3
      U1 = U(:,i); U2 = U(:,j);
```

```
      qe{i,j} = reshape(sum((U1(edofMat)*KE).*U2(edofMat),2),nely,nelx)/(nelx*nely);
      Q(i,j) = sum(sum((Emin+xPhys.^penal*(E0-Emin)).*qe{i,j}));
      dQ{i,j} = penal*(E0-Emin)*xPhys.^(penal-1).*qe{i,j};
    end
  end
  c = -(Q(1,1)+Q(2,2)+Q(1,2)+Q(2,1));
  dc = -(dQ{1,1}+dQ{2,2}+dQ{1,2}+dQ{2,1});
  dv = ones(nely,nelx);
  %% FILTERING/MODIFICATION OF SENSITIVITIES
  if ft == 1
    dc(:) = H*(x(:).*dc(:))./Hs./max(1e-3,x(:));
  elseif ft == 2
    dc(:) = H*(dc(:)./Hs);
    dv(:) = H*(dv(:)./Hs);
  end
  %% OPTIMALITY CRITERIA UPDATE OF DESIGN VARIABLES AND PHYSICAL DENSITIES
  l1 = 0; l2 = 1e9; move = 0.2;
  while (l2-l1 > 1e-9)
    lmid = 0.5*(l2+l1);
    xnew = max(0,max(x-move,min(1,min(x+move,x.*sqrt(-dc./dv/lmid)))));
    if ft == 1
      xPhys = xnew;
    elseif ft == 2
      xPhys(:) = (H*xnew(:))./Hs;
    end
    if mean(xPhys(:)) > volfrac, l1 = lmid; else l2 = lmid; end
  end
  change = max(abs(xnew(:)-x(:)));
  x = xnew;
  %% PRINT RESULTS
  fprintf(' It.:%5i Obj.:%11.4f Vol.:%7.3f ch.:%7.3f\n',loop,c, mean(xPhys(:)),change);
  %% PLOT DENSITIES
  colormap(gray); imagesc(1-xPhys); caxis([0 1]); axis equal; axis off; drawnow;
end
```

References

Allaire G, Jouve F, Toader AM (2004) Structural optimization using sensitivity analysis and a level-set method. J Comput Phys 194(1):363–393

Almeida SRM, Paulino GH, Silva ECN (2010) Layout and material gradation in topology optimization of functionally graded structures: a global-local approach. Struct Multidiscip Optim 42(6):855–868

Amstutz S, Giusti S, Novotny A, De Souza Neto E (2010) Topological derivative for multi-scale linear elasticity models applied to the synthesis of microstructures. Int J Numer Methods Eng 84(6):733–756

Andreassen E, Clausen A, Schevenels M, Lazarov BS, Sigmund O (2011) Efficient topology optimization in matlab using 88 lines of code. Struct Multidiscip Optim 43(1):1–16

Andreassen E, Lazarov B, Sigmund O (2014) Design of manufacturable 3d extremal elastic microstructure. Mech Mater 69:1–10

Bendsøe MP, Kikuchi N (1988) Generating optimal topologies in structural design using a homogenization method. Comput Methods Appl Mech Eng 71(2):197–224

Bendsøe MP, Sigmund O (2003) Topology optimization: theory, methods and applications. Springer, Berlin

Challis VJ (2010) A discrete level-set topology optimization code written in matlab. Struct Multidiscip Optim 41(3):453–464

Challis VJ, Roberts AP, Wilkins AH (2008) Design of three dimensional isotropic microstructures for maximized stiffness and conductivity. Int J Solids Struct 45(14–15):4130–4146

Gibiansky L, Sigmund O (2000) Multiphase composites with extremal bulk modulus. J Mech Phys Solids 48(3):461–498

Guedes J, Kikuchi N (1990) Preprocessing and postprocessing for materials based on the homogenization method with adaptive finite element methods. Comput Methods Appl Mech Eng 83(2):143–198

Guest JK, Prévost JH (2007) Design of maximum permeability material structures. Comput Methods Appl Mech Eng 196(4–6):1006–1017

Hashin Z (1983) Analysis of composite materials—a survey. J Appl Mech Trans ASME 50(3):481–505

Hassani B, Hinton E (1998b) A review of homogenization and topology opimization ii—analytical and numerical solution of homogenization equations. Comput Struct 69(6):719–738

Huang X, Xie YM (2010) A further review of eso type methods for topology optimization. Struct Multidiscip Optim 41(5):671–683

Huang X, Radman A, Xie YM (2011) Topological design of microstructures of cellular materials for maximum bulk or shear modulus. Comput Mater Sci 50(6):1861–1870

Liu Z, Korvink J, Huang R (2005) Structure topology optimization: fully coupled level set method via femlab. Struct Multidiscip Optim 29(6):407–417

Mahdavi A, Balaji R, Frecker M, Mockensturm EM (2006) Topology optimization of 2d continua for minimum compliance using parallel computing. Struct Multidiscip Optim 32(2):121–132

Michel JC, Moulinec H, Suquet P (1999) Effective properties of composite materials with periodic microstructure: a computational approach. Comput Methods Appl Mech Eng 172(1–4):109–143

Neves MM, Rodrigues H, Guedes JM (2000) Optimal design of periodic linear elastic microstructures. Comput Struct 76(1):421–429

Paulino GH, Silva ECN, Le CH (2009) Optimal design of periodic functionally graded composites with prescribed properties. Struct Multidiscip Optim 38(5):469–489

Rodrigues H, Guedes JM (2002) Hierarchical optimization of material and structure. Struct Multidiscip Optim 24(1):1–10

Sigmund O (1994) Materials with prescribed constitutive parameters: an inverse homogenization problem. Int J Solids Struct 31(17):2313–2329

Sigmund O (2000) New class of extremal composites. J Mech Phys Solids 48(2):397–428

Sigmund O (2001) A 99 line topology optimization code written in matlab. Struct Multidiscip Optim 21(2):120–127

Sigmund O (2007) Morphology-based black and white filters for topology optimization. Struct Multidiscip Optim 33(4–5):401–424

Sigmund O, Maute K (2013) Topology optimization approaches—a comparative review. Struct Multidiscip Optim 48(6):1031–1055

Sigmund O, Torquato S (1997) Design of materials with extreme thermal expansion using a three-phase topology optimization method. J Mech Phys Solids 45(6):1037–1067

Suresh K (2010) A 199-line matlab code for pareto-optimal tracing in topology optimization. Struct Multidiscip Optim 42(5):665–679

Svanberg K (1987) Method of moving asymptotes—a new method for structural optimization. Int J Numer Methods Eng 24(2):359–373

Talischi C, Paulino G, Pereira A, Menezes I (2012a) Polymesher: a general-purpose mesh generator for polygonal elements written in matlab. Struct Multidiscip Optim 45(3):309–328

Talischi C, Paulino GH, Pereira A, Menezes IFM (2012b) Polytop: a matlab implementation of a general topology optimization framework using unstructured polygonal finite element meshes. Struct Multidiscip Optim 45(3):329–357

Wang Y, Luo Z, Zhang N, Kang Z (2014) Topological shape optimization of microstructural metamaterials using a level set method. Comput Mater Sci 87:178–186

Xia L, Breitkopf P (2014a) Concurrent topology optimization design of material and structure within fe^2 nonlinear multiscale analysis framework. Comput Methods Appl Mech Eng 278:524–542

Xia L, Breitkopf P (2014b) A reduced multiscale model for nonlinear structural topology optimization. Comput Methods Appl Mech Eng 280:117–134

Xia L, Breitkopf P (2015) Multiscale structural topology optimization with an approximate constitutive model for local material microstructure. Comput Methods Appl Mech Eng 286:147–167

Xia Z, Zhang Y, Ellyin F (2003) A unified periodical boundary conditions for representative volume elements of composites and applications. Int J Solids Struct 40(8):1907–1921

Xia Z, Zhou C, Yong Q, Wang X (2006) On selection of repeated unit cell model and application of unified periodic boundary conditions in micro-mechanical analysis of composites. Int J Solids Struct 43(2):266–278

Xia L, Zhu J, Zhang W (2012) A superelement formulation for the efficient layout design of complex multi-component system. Struct Multidiscip Optim 45(5):643–655

Xia L, Zhu J, Zhang W, Breitkopf P (2013) An implicit model for the integrated optimization of component layout and structure topology. Comput Methods Appl Mech Eng 257:87–102

Yin L, Yang W (2001) Optimality criteria method for topology optimization under multiple constraints. Comput Struct 79(20–21):1839–1850

Zhang W, Sun S (2006) Scale-related topology optimization of cellular materials and structures. Int J Numer Methods Eng 68(9):993–1011

Zhang W, Dai G, Wang F, Sun S, Bassir H (2007) Using strain energy-based prediction of effective elastic properties in topology optimization of material microstructures. Acta Mech Sinica/Lixue Xuebao 23(1):77–89